Advances in Water Resources 112 (2018) 95–105

Contents lists available at ScienceDirect

Advances in Water Resources

journal homepage: www.elsevier.com/locate/advwatres

An advanced analytical solution for pressure build-up during CO_2 injection into infinite saline aquifers: The role of compressibility

Wu Haiqing, Bai Bing*, Li Xiaochun

State Key Laboratory of Geomechanics and Geotechnical Engineering, Institute of Rock and Soil Mechanics, Chinese Academy of Sciences, Wuhan, Hubei 430071, China

ARTICLE INFO

Keywords:
Analytical solution
Compressibility
CO_2-brine flow
Relative permeability
CO_2 geological storage

ABSTRACT

Existing analytical or approximate solutions that are appropriate for describing the migration mechanics of CO_2 and the evolution of fluid pressure in reservoirs do not consider the high compressibility of CO_2, which reduces their calculation accuracy and application value. Therefore, this work first derives a new governing equation that represents the movement of complex fluids in reservoirs, based on the equation of continuity and the generalized Darcy's law. A more rigorous definition of the coefficient of compressibility of fluid is then presented, and a power function model (PFM) that characterizes the relationship between the physical properties of CO_2 and the pressure is derived. Meanwhile, to avoid the difficulty of determining the saturation of fluids, a method that directly assumes the average relative permeability of each fluid phase in different fluid domains is proposed, based on the theory of gradual change. An advanced analytical solution is obtained that includes both the partial miscibility and the compressibility of CO_2 and brine in evaluating the evolution of fluid pressure by integrating within different regions. Finally, two typical sample analyses are used to verify the reliability, improved nature and universality of this new analytical solution. Based on the physical characteristics and the results calculated for the examples, this work elaborates the concept and basis of partitioning for use in further work.

1. Introduction

Investigations into the theory of multiphase flow in porous media originated in the exploitation of oil and gas resources. It has been shown by many years of engineering practice that the actual flow that is present during the process of exploitation of oil fields under conditions of saturated vapor pressure or with injection of water is two-phase flow involving oil-gas or oil-water (Kong, 2010). Therefore, the theory of multiphase flow was established gradually beginning in the 1930s. In this area, the most classic analytical solution is the particular solution for two phase flow in one dimension that was solved by Buckley and Leverett (1942), according to the method of characteristics, assuming incompressible and immiscible flow and no capillary pressure. It has been verified by ample practical engineering applications (Blunt and King, 1991; Kong, 2010). The relevant fluids are mainly incompressible or slightly compressible oil, water, natural gas, etc. in the traditional exploitation of oil and gas. They are immiscible and the capillary pressure is also small, so that the assumptions of the above analytical solution are basically appropriate (Kong, 2010).

However, in the most recent twenty years, oil and gas resources have become increasingly depleted, and traditional oil and gas resources and exploitation patterns cannot meet the demand of human development for energy. Therefore, some scholars have proposed a new exploitation method that involves injecting gas (nitrogen) to enhance the recovery efficiency of oil and gas resources (Johns et al., 2002; Taber et al., 1997), and new underground resources of shale gas (Cooper et al., 2016; Golding et al., 2013), condensate gas (Li et al., 2012), etc., have been discovered. Moreover, the demand for CO_2 (the main greenhouse gas causing global warming) storage is becoming increasingly large because of the increasingly deteriorated environment (IPCC, 2005). Many investigations have suggested that CO_2 geological storage is the most effective method of sequestration (Bachu, 2000; Lal, 2008; Michael et al., 2010). Subsequently, the concept and method of exploiting underground resources of oil, gas, geothermal energy, etc. by injecting CO_2 and realizing CO_2 storage at the same time has obtained general support among scholars, considering the economic costs (Alvarado and Manrique, 2010; Damen et al., 2005; Gozalpour et al., 2005; Nagy and Olajossy, 2008; Poordad and Forutan, 2013; Pruess, 2006; Wojnarowski, 2012). Hence, the main fluids are CO_2-brine or CO_2-oil in this new kind of engineering. However, it is not known whether the traditional analytical solutions for multiphase flow are valid because of the particularity of CO_2. Consequently, the physical

* Corresponding author.
E-mail address: bai_bing2@126.com (B. Bai).

https://doi.org/10.1016/j.advwatres.2017.12.010
Received 17 May 2017; Received in revised form 1 November 2017; Accepted 8 December 2017
Available online 09 December 2017
0309-1708/

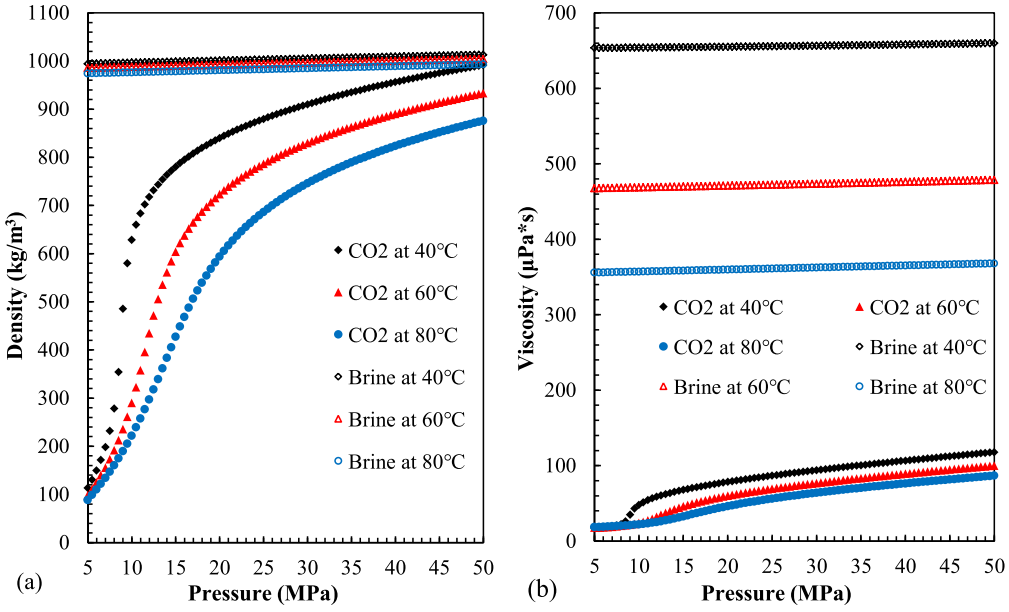

Fig. 1. State curves of the physical properties of CO_2 and brine as a function of pressure ((a): density; (b): viscosity). Data taken from the NIST (National Institute of Standards and Technology, USA) Chemistry WebBook (2016).

properties of CO_2 have been studied in many ways (Fenghour et al., 1998; Span and Wagner, 1996; Vesovic et al., 1990). The results show that the phase diagram of CO_2 is very special, compared with water and other gases. With changes in pressure and temperature, CO_2 can reach a supercritical state, in addition to the conventional three states of gas, liquid, and solid. When the pressure and temperature approach the critical point (7.38 MPa, 31.1 ˚C), the physical properties of CO_2 are very different (Span and Wagner, 1996). Fig. 1 shows the state curves of the physical properties of CO_2 and brine as a function of pressure ((a): density; (b): viscosity). It is clear that CO_2 has properties including high compressibility, low viscosity and low density compared with water. Therefore, the traditional assumption of an incompressible fluid described above is inappropriate. In addition, CO_2 is also partially miscible in brine (Dilmore et al., 2006; Lu et al., 2008).

Generally, to consider the complicated physical properties of CO_2, scholars prefer to apply numerical methods to explore the migration mechanics of CO_2 plumes and the evolution of fluid pressure in reservoirs (Pruess, 2005; Zyvoloski, 2007). However, the numerical method is very dependent on the availability of a high performance electronic computer, and problems often occur during the solution process. These problems include numerical oscillations, non-convergence and low efficiency. Therefore, sometimes the analytical method reflecting the physical essence of flow may be a better choice (Mathias et al., 2009; Mijic et al., 2014; Wu et al., 2016). In terms of analytical methods, many scholars have done considerable work in the area of CO_2 geological storage (Celia et al., 2015; Mijic et al., 2014). The work of Nordbotten and his research group (Nordbotten and Celia, 2006a,b; Nordbotten et al., 2005a,b) is most representative. They obtained a continuous function that represents the thickness of CO_2 plume based on the principle of energy minimization, and then proposed some semi-analytical solutions and approximate solutions. Subsequently, it was further developed by other scholars (Azizi and Cinar, 2013; Cihan et al., 2013; Mathias et al., 2009; Mathias et al., 2011a; Mathias et al., 2011b; Vilarrasa et al., 2013). Whereas, only the partial miscibility of CO_2 and brine is considered in the above work and it is limited to semi-analytical solutions or approximate solutions (Wu et al., 2016). More recently, Wu et al. (2016) developed an explicit integral solution by directly integrating the governing equation of fluid migration in the reservoir. The process of solution did not involve any numerical method, it is a pure analytical solution that considers the partial miscibility of CO_2 and brine. However, as to the compressibility of fluid, which has a great of impact on the evolution of fluid pressure in the reservoir for the high compressible fluid media, no breakthroughs at all exist in present analytical work. It should be noted that minority scholars (Mijic et al., 2014; Nordbotten and Celia, 2006b; Vilarrasa et al., 2010) presented some iterative algorithms for treating compressibility, although they are separated from the essence of the analytical method. The most pressing problem is that the variation in the density and viscosity of CO_2 under different pressures and temperatures is very considerable; however the appropriate function to characterize this complicated relationship has not yet been derived. Therefore, when considering the compressibility of fluid, the only applicable method to update the parameters of the fluid involves establishing a data base (Pruess, 2005; Zyvoloski, 2007), so that it transforms into a numerical solution method.

To solve the above problem regarding the compressibility of fluid, this work first describes the problem clearly and presents the basic assumptions applied in this article before presenting the following three innovative studies. In Section 3, we derive a new governing equation that describes the movement of complex fluids in reservoirs by combining the equation of continuity, including the compressibility of fluid, with the formulation of Darcy's law generalized to multiphase flows. In Section 4, we define a new coefficient of compressibility using the basic concept of compressibility. The power function model characterizing the relationship between the physical properties of CO_2 and pressure is then deduced. In Section 5, we apply the power function model to the above governing equation and obtain an advanced analytical solution, including the compressibility of fluid, for the evolution of fluid pressure in the reservoir by integrating within different regions. Finally, we analyze two typical examples to verify the reliability, improved nature and universality of this work by comparing the calculated results from this advanced analytical solution with the results of previous analytical solutions and simulated results from TOUGH2/ECO2N.

2. Problem description and basic assumptions

To express the problem clearly and conveniently, this work subsequently takes a two-phase flow involving CO_2-brine as an example to establish an analytical solution for fluid pressure evolution in the reservoir. The corresponding practical projects are mainly CO_2 geological storage and CO_2-enhanced geothermal systems. In these projects, CO_2 is generally injected into the target reservoirs through injection wells at a constant mass injection rate (Bai et al., 2017; Wu et al., 2017). As the reservoirs are completely saturated with brine in their natural state, the

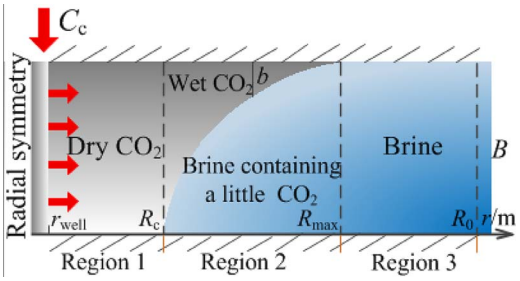

Fig. 2. Schematic profile of CO_2 and brine flow in the reservoir (r_{well} is the radius of the injection well [L]; R_c and R_{max} are the maximum radiuses of the CO_2 plume at the bottom and top of the reservoir [L], respectively; and R_0 is the maximum radius that the flow influences in the reservoir [L], which corresponds to the outer boundary; and b and B are the thicknesses of the CO_2 plume and the reservoir [L], respectively).

actual migration of the injected CO_2 is a process by which the CO_2 continuously displaces the brine. However, the density of CO_2 is smaller than that of the brine, as shown in Fig. 1, which induces an apparent phenomenon of buoyancy; thus, the CO_2 is concentrated at the tops of reservoirs (Nordbotten et al., 2005a). In the flow field of the injected CO_2, CO_2 co-exists with brine in each pore, and they will form separate flow channels by each other because the CO_2 and brine are only partially miscible (Kong, 2010). The ratios of CO_2 and brine are expressed by their saturations at one point, and the saturation of CO_2 increases gradually while it decreases for brine during the same process, as the displacement develops (Wu et al., 2016). Therefore, from a macroscopic point of view, a schematic profile of CO_2 and brine flow in the reservoir like that shown in Fig. 2 is completely different from the piston-like displacement (Kong, 2010) in traditional oil and gas fields.

To describe the actual process of displacement using mathematical models, some necessary constraining conditions are needed. The main basic assumptions applied in this work are as follows.

(1) A homogeneous and isotropic reservoir without a hydraulic gradient in its natural state extends infinitely in the horizontal direction and is overlain and underlain by thick, impervious rocks.
(2) The flow is steady and isothermal two phase flow. Given that the depths of the target reservoirs are greater than 800 m, the temperature of any given reservoir is relatively high and steady (Bachu, 2000, 2003). Thus, the actual flow in the reservoir can be regarded as an isothermal process, if the injection rate is not particularly large. Though displacement is essentially an unsteady movement because the saturation, density and viscosity of the fluids are all changing, it can be considered as a steady flow to permit consideration of the homogeneous and infinite reservoir under a constant injection rate (Nordbotten et al., 2005a).
(3) The vertical pressure gradient and the capillary pressure in the reservoir are neglected.
(4) Chemical reactions are not considered.
(5) The reservoir is saturated at all points. There is a sharp interface between the CO_2 and the brine; the CO_2 domain exists on one side of the interface, whereas the brine domain exists on the other side (Nordbotten et al., 2005a). As injection time increases, the interface extends outward gradually and the whole flow field presents three regions with different characteristics. The partial miscibility of CO_2 and brine is considered by the saturation of fluids in region 2 (Wu et al., 2016). The former half of this assumption was proposed by Nordbotten et al. (2005a); subsequently, they developed the assumption of two interfaces to consider the residual saturation of brine (Nordbotten and Celia, 2006b). While the physical concept is very clear, it causes great difficulties for the mathematical model, and the partial CO_2 dissolved into brine at the CO_2 front is still not included (Mathias et al., 2011a; Wu et al., 2016). Therefore, Wu et al. (2016) abandoned the multi-interface assumption and developed the latter half of this assumption, subsequently obtaining a pure analytical solution that not only includes the residual saturation of brine but also considers the partial dissolution of CO_2 into brine. Therefore, that assumption is also applied in this article, so that the final analytical solution can consider both the partial miscibility and the compressibility of CO_2 and brine. Noting that the above three regions in Fig. 2 are not fully agreement with the three domains (CO_2 domain, brine domain 1 and brine domain 2) of Wu et al. (2016) in geometry, although the Fig. 2 here is similar to that of Wu et al. (2016). Specifically, CO_2 domain includes the region 1 and a part of region 2, while the brine domain 1 only is a part of region 2. The physical difference of that is the residual brine distributes in the whole CO_2 domain in Wu et al. (2016), while it only distributes in a part of region 2 in this work because the residual brine of region 1 will evaporates and then migrates into the region 2. It will be elaborated further in Section 5.

3. Mathematical model

As mentioned previously, the pores of the porous medium are all saturated with fluids, and each fluid phase has its separate flow channel. Thus, the equation of continuity describing the multiphase flow of complex fluids in the reservoir can be expressed by,

$$\frac{\partial(\rho_\alpha \phi S_\alpha)}{\partial t} + \nabla\cdot(\rho_\alpha \mathbf{V}_\alpha) = 0 \tag{1}$$

$$\sum S_\alpha = 1 \tag{2}$$

where ρ is the density of the fluid [ML^{-3}]; ϕ is the porosity of the reservoir; S denotes the saturation of the fluid; t is injection time [T]; and $\mathbf{V}$ is a tensor of Darcy velocity [LT^{-1}]. The subscript α identifies each fluid, with α = c for CO_2 and α = w for brine in this article.

As the upper and lower boundaries are both thick impervious rock layers, they can be regarded as zero flow boundaries (the second kind of boundary). The reservoir extends infinitely in the radial direction, so the remote outer boundary is a constant pressure boundary, which is consistent with the initial formation pressure, and its location is a function of time. Therefore, the outer boundary conditions are,

$$\begin{cases} \frac{\partial P}{\partial n}\Big|_{\text{Upper and lower boundaries}} = 0 \\ P_{R_0} = P_0 \end{cases} \tag{3}$$

where P is the vertically averaged fluid pressure in the reservoir [$ML^{-1}T^{-2}$]; n is the direction normal to the upper and lower boundaries of the reservoir; P_{R_0} is the vertically averaged fluid pressure at the location of R_0; and P_0 is the initial formation pressure.

In addition, there is an inner boundary in the reservoir, i.e., the injection well. It can be considered as a source term or inner boundary when establishing the flow model (Kong, 2010). The latter is adopted here to ease the derivation of the model, as shown in Eq. (4),

$$\rho\frac{k}{\mu}\frac{\partial P}{\partial r}\Big|_{r_{well}} = -\frac{C_c}{2\pi r_{well} B} \tag{4}$$

where k is the absolute permeability of the reservoir [L^2]; μ is the viscosity of the fluid [$ML^{-1}T^{-1}$]; r is the radial distance far from the center of the wellbore [L]; and C_c is the mass injection rate [MT^{-1}].

The initial condition is,

$$P(r, t = 0) = P_0 \tag{5}$$

For steady two phase flow, Eq. (1) can be simplified to,

$$\nabla\cdot(\rho_c \mathbf{V}_c + \rho_w \mathbf{V}_w) = 0 \tag{6}$$

Furthermore, as the homogeneous and isotropic reservoir extends infinitely in the horizontal direction, the radial Darcy velocity of the fluid is radially symmetric. Hence, in cylindrical coordinates, Eq. (6) can be transformed into,

$$\frac{1}{r}\frac{\partial}{\partial r}(r\rho_c v_{rc} + r\rho_w v_{rw}) = 0 \tag{7}$$

where v_r is the radial Darcy velocity of the fluid [LT^{-1}].

Integrating Eq. (7), we have,

$$r(\rho_c v_{rc} + \rho_w v_{rw}) = \text{Const.} \tag{8}$$

Taking the relative permeability to represent the athletic ability of each fluid phase in the reservoir, the radial Darcy velocity of the fluid is,

$$v_{r\alpha} = -\frac{kk_{r\alpha}}{\mu_\alpha}\frac{dP}{dr} \tag{9}$$

Bringing Eq. (9) into Eq. (8),

$$-rk\left(\rho_c\frac{k_{rc}}{\mu_c} + \rho_w\frac{k_{rw}}{\mu_w}\right)\frac{dP}{dr} = \text{Const.} \tag{10}$$

where k_r is the relative permeability of the fluid.

Importing the inner boundary condition represented by Eq. (2), we obtained Const. $= C_c/2\pi B$. Thus, the governing equation that includes the compressibility of the fluid and depicts the movement of complex fluids in a reservoir is,

$$-\left(\rho_c\frac{k_{rc}}{\mu_c} + \rho_w\frac{k_{rw}}{\mu_w}\right)\frac{dP}{dr} = \frac{C_c}{2\pi rkB} \tag{11}$$

Since $\upsilon = \mu/\rho$, Eq. (11) can also be expressed as,

$$-\left(\frac{k_{rc}}{\upsilon_c} + \frac{k_{rw}}{\upsilon_w}\right)\frac{dP}{dr} = \frac{C_c}{2\pi rkB} \tag{12}$$

where υ is the kinematic viscosity of the fluid [L^2T^{-1}].

4. Coefficient of compressibility

As the physical properties of fluids are functions of pressure for isothermal flow (Kong, 2010), to solve the above governing equation by analytical methods, the density and viscosity or kinematic viscosity of the fluid must be expressed as explicit functions of pressure. As shown in Fig. 1, the changes in the density and viscosity of brine are very small as pressure increases, so these quantities can be considered to be constants. For CO_2, though, the differences in density and viscosity under different pressure are very great, although rapid changes only occur near the critical point. When the pressure approaches a certain value (which changes with temperature; for example, it is approximately 20 MPa for 60 °C), the relationship between the density and viscosity of CO_2 and the pressure satisfies some type of function. The conclusions of Bachu (2003) indicate that the depths of target reservoirs are relatively large, so that the temperature of the target reservoir is higher than 40 °C, and the initial formation pressure is larger than 12 MPa. Therefore, after CO_2 is injected into the reservoir, it is in a supercritical state. Therefore, it is appropriate to use a type of function to characterize the density and viscosity of CO_2 within a certain pressure interval, from the viewpoint of engineering demands.

In traditional treatments of seepage mechanics in porous media, the coefficient of compressibility of a fluid is defined as (Kong, 2010),

$$c_f = -\frac{1}{V}\frac{dV}{dP} \tag{13}$$

where c_f is the traditional coefficient of compressibility of the fluid [$ML^{-1}T^{-2}$]; and V is the volume of the fluid [L^3]. The negative sign means that the volume decreases as pressure increases.

On the basis of Eq. (13), an exponential function model (EFM) for density can be deduced,

$$\rho = \rho_0 e^{c_{f\rho}(P-P_0)} \tag{14}$$

where ρ_0 is the original density of the fluid corresponding to P_0 [ML^{-3}]; and $c_{f\rho}$ is the coefficient of compressibility of the fluid in terms of density [$ML^{-1}T^{-2}$].

Similarly, EFMs describing the viscosity and kinematic viscosity can be obtained,

$$\mu = \mu_0 e^{c_{f\mu}(P-P_0)} \tag{15}$$

$$\upsilon = \upsilon_0 e^{c_{f\upsilon}(P-P_0)} \tag{16}$$

where μ_0[$ML^{-1}T^{-1}$] and υ_0[L^2T^{-1}] are the original viscosity and the original kinematic viscosity of the fluid corresponding to P_0, respectively; and $c_{f\mu}$[$ML^{-1}T^{-2}$] and $c_{f\upsilon}$[$ML^{-1}T^{-2}$] are the coefficients of compressibility of the fluid for viscosity and kinematic viscosity, respectively.

Moreover, the above three coefficients of compressibility satisfy the following relationship, so if two of them are known, the third can be determined.

$$c_{f\upsilon} = c_{f\mu} - c_{f\rho} \tag{17}$$

However, it can be found that the density and viscosity of supercritical CO_2 do not rise in a way that follows the form of an exponential function as pressure increases; the actual rate of rise decreases gradually, according to Fig. 1. Therefore, the traditional definition of the coefficient of compressibility is inappropriate, especially for CO_2. Analyzing Eq. (13) from a mathematical perspective, a problem can be found in that the traditional definition adopts the ratio of the volumetric relative change to the absolute change of pressure, which is not enough scientific in mathematics. A more rigorous definition about the coefficient of compressibility would be,

$$c_f' = -\frac{dV}{V}/\frac{dP}{P} \tag{18}$$

where c_f' is the new coefficient of compressibility of a fluid defined by this work.

Hence, the power function model (PFM) describing the density, viscosity and kinematic viscosity can be derived,

$$\begin{cases} \rho = \rho_0(P/P_0)^{c_{f\rho}'} \\ \mu = \mu_0(P/P_0)^{c_{f\mu}'} \\ \upsilon = \upsilon_0(P/P_0)^{c_{f\upsilon}'} \end{cases} \tag{19}$$

where $c_{f\rho}'$, $c_{f\mu}'$ *and* $c_{f\upsilon}'$ are the new coefficients describing the compressibility of fluids with respect to density, viscosity and kinematic viscosity, respectively.

Similarly, the three new coefficients of compressibility satisfy Eq. (20),

$$c_{f\upsilon}' = c_{f\mu}' - c_{f\rho}' \tag{20}$$

Here, taking the data of NIST Chemistry WebBook (2016) as standard, we compared it with the results predicted using the EFM and the PFM for density, viscosity and kinematic viscosity to verify which definition of the coefficient of compressibility is more reliable and appropriate. We adopt the three different temperatures shown in Fig. 1 (40 °C, 60 °C, and 80 °C), and the corresponding pressure intervals are 15–35 MPa, 20–40 MPa and 25–45 MPa, respectively. The original pressure under different temperatures is close to the corresponding initial formation pressure, so the results can be applied in engineering applications directly. Table 1 shows the values of coefficients of compressibility in the EFM and PFM under different temperatures, and the comparison of predicted results are shown in Fig. 3 and Table 2. Meanwhile, considering Eq. (12), the kinematic viscosity of brine under different pressures are also shown in Fig. 3.

Based on Fig. 3, it is clear that the results predicted by the PFM are more consistent with the NIST data, compared with the results predicted by the EFM. In addition, the coefficients associated with the PFM are all larger than those of the EFM, according to Table 2. These results suggest that the new definition of the coefficient of compressibility can better characterize the relationship between the physical properties of

Table 1
The values of coefficients of compressibility for the EFM and PFM under different temperatures.

T (°C)	EFM			PFM		
	$c_{f\rho}$ (1/Pa)	$c_{f\mu}$ (1/Pa)	$c_{f\upsilon}$ (1/Pa)	$c'_{f\rho}$	$c'_{f\mu}$	$c'_{f\upsilon}$
40	1.05×10^{-8}	2.2×10^{-8}	1.15×10^{-8}	0.21	0.46	0.25
60	1.15×10^{-8}	2.15×10^{-8}	1×10^{-8}	0.31	0.58	0.27
80	1.25×10^{-8}	2.1×10^{-8}	8.5×10^{-9}	0.36	0.63	0.27

Table 2
The coefficient of association (R^2) between the results predicted by the EFM and the PFM and the data of NIST Chemistry WebBook (2016).

T (°C)	R^2 of EFM			R^2 of PFM		
	Density	Viscosity	Kinematic viscosity	Density	Viscosity	Kinematic viscosity
40	0.954	0.948	0.952	0.996	0.998	0.998
60	0.956	0.951	0.961	0.985	0.989	0.998
80	0.957	0.953	0.978	0.992	0.993	0.997

fluids and pressure. Therefore, it will be applied in Section 5. As the physical properties of brine are taken to be constant, in the following text, the symbols representing the coefficients of compressibility will be the same as in Eq. (19). All these symbols denote the coefficients of compressibility of CO_2. Moreover, the rate of increase of the PFM is decreasing, as well as the increase in pressure. According to Fig. 3, these results are consistent with the actual case. Therefore, the results predicted by the PFM are still relatively ideal, even extending the interval of pressure to some extent. As Fig. 3(d) shows, the kinematic viscosity of brine is more stable than its density and viscosity. This result indicates that incorporating the density into the governing equation transforms the viscosity into the kinematic viscosity, which improves the accuracy of models, though they are all regarded as constants for brine. That is, models that include the compressibility of fluid are more reliable.

5. Solution using analytical methods

According to assumption (5) and the idea of Wu et al. (2016), during the process of injecting CO_2 to displace brine, the whole flow field can be divided into three regions, as shown in Fig. 2. Region 1 is dry CO_2. It is continuously provided with gas, inducing increases in fluid pressure, so it can be named as the gas source region. Region 2 is wet CO_2 and brine containing a little CO_2. Here, CO_2 is continuously transferred from the gas source region into region 3. It displaces the original brine at the same time, so this region is named the region of displacement. The CO_2 and brine are partially miscible and form a sharp interface in this region. Therefore, we name the two sides of the interface as the CO_2 domain and the brine domain. Region 3 contains only brine, which continuously drains away and decreases in pressure, so this region is named the region of drainage. In existing work, to solve the governing equation describing the movement of complex fluids in the reservoir by analytical methods or semi-analytical methods, the usual approach is to assume the saturation of each fluid phase in the flow field, select the relative permeability model, and finally solve the model. There is no problem for the gas source region and the region of drainage. However, with regard to the region of displacement, the approach of assuming an

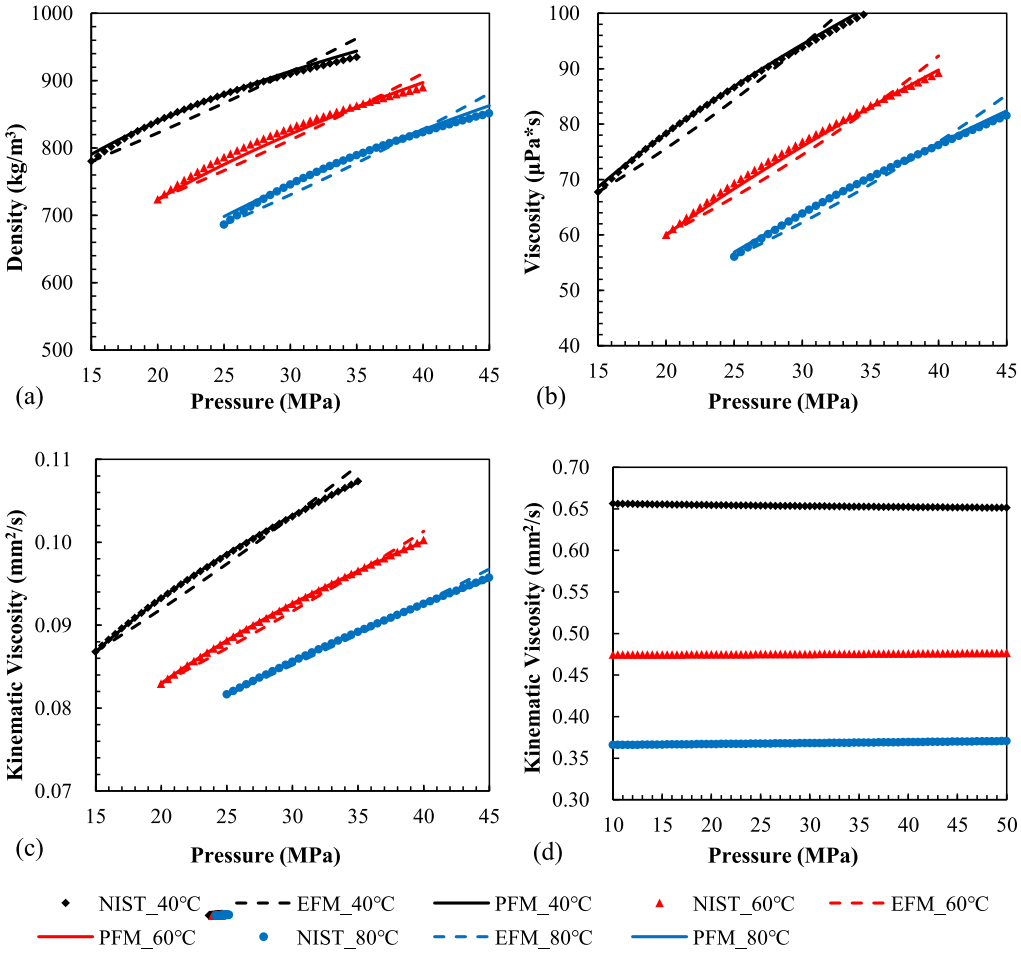

Fig. 3. Comparison of results predicted by the EFM and the PFM ((a): the density of CO_2; (b): the viscosity of CO_2; (c): the kinematic viscosity of CO_2; (d): the kinematic viscosity of brine).

average saturation based on the different fluid domains must be discussed further. The most important disadvantage is its indeterminacy; it is difficult to find the appropriate average saturation. Wu et al. (2016) presented a method for performing sensitivity analysis using various parameter combinations to determine the saturation of each fluid phase of different fluid domains in the region of displacement; however, it is random and difficult to apply.

Actually, according to the mathematical model in Section 3, the parameter necessary for solving the governing equation above is the relative permeability of each fluid phase, not their saturation. Therefore, it may be better to directly assume the relative permeability of each fluid phase in the flow field. In the gas source region, the residual brine will evaporate into the CO_2. It is then brought into the region of displacement by the CO_2 and forms the wet CO_2 in the region of displacement. Given that only CO_2 exists in the gas source region, the relative permeability of CO_2 and brine are 1 and 0, respectively. In the region of drainage, the flow is made up solely of brine, and the relative permeability of CO_2 and the brine are 0 and 1, respectively. These values are consistent with the method of assuming saturation. For the region of displacement, it is necessary to assume the relative permeability of each fluid phase, based on the different fluid domains.

Taking the region of displacement as the unit of the control body, we have $k_{rw,R_c} = 0$ and $k_{rc,R_c} = 1$ at the left side, i.e., only CO_2 is flowing into the unit; similarly, on the right side, $k_{rw,R_{max}} = 1$ and $k_{rc,R_{max}} = 0$, i.e., only brine flows out the unit. From left to right, the relative permeability of CO_2 changes gradually from 1 to 0, while the relative permeability of the brine changes from 0 to 1. Therefore, according to the theory of gradual change, the average of the relative permeability of each fluid phase at the two sides of the unit can be considered to be the average relative permeability of the unit,

$$\begin{cases} \overline{k_{rc,2}} = (k_{rc,R_c} + k_{rc,R_{max}})/2 = 0.5 \\ \overline{k_{rw,2}} = (k_{rw,R_c} + k_{rw,R_{max}})/2 = 0.5 \end{cases} \tag{21}$$

where $\overline{k_{r\alpha,x}}$ is the averaged relative permeability of a fluid at the location/region of x. The second subscript x = 1, 2, 3, 2c, 2w, R_c and R_{max}, which denote the gas source region, the region of displacement, the region of drainage, the CO_2 domain in the region of displacement, the brine domain in the region of displacement, and the location of R_c and R_{max}, respectively. Similarly, the parameters $k_{r\alpha,x}$,$S_{\alpha,x}$,$\rho_{\alpha,x}$ and so on, are all like this.

As the enriched fluid phase is the main flow in the different fluid domains, the contribution of the other fluid to the effective permeability is negligible (Kong, 2010). Hence, the averaged relative permeability of CO_2 in the CO_2 domain is equal to the averaged relative permeability of CO_2 in the region of displacement, i.e., $\overline{k_{rc,2c}} = \overline{k_{rc,2}}$. Similarly, $\overline{k_{rw,2w}} = \overline{k_{rw,2}}$. Thus, the average saturation of each fluid phase in the CO_2 domain and the brine domain can be obtained on the basis of the relative permeability model. If we bring the average saturation into the relative permeability model again, the relative permeability of the non-enriched fluid phase can be obtained, so the reliability of ignoring it can be verified. We take the Corey model (Pruess et al., 1999) as an example, setting the residual saturation of CO_2 and brine to 0.05 and 0.4, respectively. According to $\overline{k_{rc,2c}} = 0.5$ and $\overline{k_{rw,2w}} = 0.5$, we obtained $\overline{S_{w,2c}} = 0.5465$ and $\overline{S_{w,2w}} = 0.8625$, and then we have $\overline{k_{rw,2c}} = 0.005$ and $\overline{k_{rc,2w}} = 0.007$. The relative errors are 1% and 1.4%, respectively, so ignoring the relative permeability of non-enriched fluid phase leads to acceptable reliability.

Based on the above analysis, to obtain the solution to the governing equation, the method of integrating within different regions is available (Wu et al., 2016). As the given outer boundary condition is located at the right side of the region of drainage, so the order of integrating is opposite to the direction of flow, i.e., it progresses in order from the region of drainage to the region of displacement and the gas source region. Moreover, the results from the preceding region are taken as the given outer boundary conditions for the next region.

It is convenient to define the mass mobility of each fluid phase $\omega_\alpha[L^{-2}T]$ as,

$$\omega_\alpha = k_{r\alpha}\frac{\rho_\alpha}{\mu_\alpha} = \frac{k_{r\alpha}}{\upsilon_\alpha} \tag{22}$$

Within the region of drainage ($R_{max} \le r \le R_0$), only brine flow occurs, so the total mass mobility of region is equal to the mass mobility of brine, or,

$$\omega_3 = \omega_{w,3} = \frac{k_{rw,3}}{\upsilon_{w,3}} \tag{23}$$

Hence, the integral form of the above governing equation in this region is,

$$\int_P^{P_0} dP = \frac{-C_c}{2\pi kB}\int_r^{R_0}\frac{1}{r\omega_{w,3}}dr \tag{24}$$

Integrating Eq. (24), we obtain,

$$P = P_0 + \frac{C_c}{2\pi kB\omega_{w,3}}\ln\frac{R_0}{r} \tag{25}$$

Therefore, the fluid pressure at R_{max} is,

$$P_{R_{max}} = P_0 + \frac{C_c}{2\pi kB\omega_{w,3}}\ln\frac{R_0}{R_{max}} \tag{26}$$

For the region of displacement ($R_c \le r < R_{max}$), as shown in Fig. 2, the CO_2 domain and the brine domain both exist at any given location, so the total mass mobility of the complex fluid is,

$$\omega_2 = \frac{b}{B}(\omega_{c,2c} + \omega_{w,2c}) + \frac{B-b}{B}(\omega_{c,2w} + \omega_{w,2w}) \tag{27}$$

As the relative permeability of the non-enriched fluid phases is negligible compared with the enriched fluid phase within different fluid domains, Eq. (27) can be simplified to,

$$\omega_2 = \frac{b}{B}\omega_{c,2c} + \frac{B-b}{B}\omega_{w,2w} \tag{28}$$

The interface between the CO_2 domain and the brine domain satisfies the following continuous function, which was derived by Nordbotten et al. (2005a) based on the principle of energy minimization and the calculus of variations. Expressing it in terms of mass mobility leads to,

$$b = \frac{B}{(\omega_{c,2c} - \omega_{w,2w})}\left(\sqrt{\frac{\omega_{c,2c}\omega_{w,2w}M_c}{\phi\pi Br^2\rho_c}} - \omega_{w,2w}\right) \tag{29}$$

where

$$M_c = \int_0^t C_c dt \tag{30}$$

where M_c is the total mass injection flux [M].

According to Eq. (28) and Eq. (29), we have,

$$\omega_2 = \sqrt{\frac{\omega_{c,2c}\omega_{w,2w}M_c}{\phi\pi Br^2\rho_c}} = \sqrt{\frac{\overline{k_{rc,2c}}\omega_{w,2w}M_c}{\phi\pi Br^2\mu_c}} \tag{31}$$

Bringing the PFM describing the density of CO_2 into Eq. (31),

$$\omega_2 = \sqrt{\frac{\overline{k_{rc,2c}}\omega_{w,2w}M_c}{\phi\pi Br^2\mu_{c,R_{max}}\left(\frac{P}{P_{R_{max}}}\right)^{c'_{\mu}}}} = \sqrt{\frac{\omega_{c,R_{max}}\omega_{w,2w}M_c}{\phi\pi Br^2\rho_{c,R_{max}}}}\left(\frac{P}{P_{R_{max}}}\right)^{\frac{-c'_{\mu}}{2}} \tag{32}$$

Substituting Eq. (32) into the governing equation, we obtain,

$$\int_P^{P_{R_{max}}}\left(\frac{P}{P_{R_{max}}}\right)^{\frac{-c'_{\mu}}{2}}dP = \frac{-C_c}{2\pi kB}\int_r^{R_{max}}\sqrt{\frac{\phi\pi B\rho_{c,R_{max}}}{\omega_{c,R_{max}}\omega_{w,2w}M_c}}dr \tag{34}$$

Integrating Eq. (34), we have,

$$P = P_{R_{\max}}\left[1 + \frac{C_c(2-c'_{f\mu})}{4\pi kBP_{R_{\max}}}\sqrt{\frac{\phi\pi B\rho_{c,R_{\max}}}{\omega_{c,R_{\max}}\omega_{w,2w}M_c}}(R_{\max}-r)\right]^{\frac{2}{2-c'_{f\mu}}} \quad (35)$$

Therefore, the fluid pressure at the location of R_c is,

$$P_{R_c} = P_{R_{\max}}\left[1 + \frac{C_c(2-c'_{f\mu})}{4\pi kBP_{R_{\max}}}\sqrt{\frac{\phi\pi B\rho_{c,R_{\max}}}{\omega_{c,R_{\max}}\omega_{w,2w}M_c}}(R_{\max}-R_c)\right]^{\frac{2}{2-c'_{f\mu}}} \quad (36)$$

The gas source region ($r_{well} \le r < R_c$) is similar to the region of drainage. Only CO_2 flow occurs here, and the mass mobility of this region is,

$$\omega_1 = \omega_{c,1} = \frac{k_{rc,1}}{\upsilon_{c,R_c}}\left(\frac{P}{P_{R_c}}\right)^{-c'_{f\upsilon}} = \omega_{c,R_c}\left(\frac{P}{P_{R_c}}\right)^{-c'_{f\upsilon}} \quad (37)$$

Incorporating this relation into the governing equation, the integral form of the governing equation in this region can be deduced; that is,

$$\int_P^{P_{R_c}}\left(\frac{P}{P_{R_c}}\right)^{-c'_{f\upsilon}}dP = \frac{-C_c}{2\pi kB}\int_r^{R_c}\frac{1}{r\omega_{c,R_c}}dr \quad (38)$$

Integrating Eq. (38), we have,

$$P = P_{R_c}\left[1 + \frac{C_c(1-c'_{f\upsilon})}{2\pi kB\omega_{c,R_c}P_{R_c}}\ln\frac{R_c}{r}\right]^{\frac{1}{1-c'_{f\upsilon}}} \quad (39)$$

Therefore, the fluid pressure located at the wall of wellbore is,

$$P_k = P_{R_c}\left[1 + \frac{C_c(1-c'_{f\upsilon})}{2\pi kB\omega_{c,R_c}P_{R_c}}\ln\frac{R_c}{r_{well}}\right]^{\frac{1}{1-c'_{f\upsilon}}} \quad (40)$$

In conclusion, the fluid pressure at any time and at any position within the reservoir can be solved using the following analytically derived equation.

$$P = \begin{cases} P_{R_c}\left[1 + \frac{C_c\left(1-c'_{f\upsilon}\right)}{2\pi kB\omega_{c,R_c}P_{R_c}}\ln\frac{R_c}{r}\right]^{\frac{1}{1-c'_{f\upsilon}}}, & r_{well} \le r < R_c \\ P_{R_{\max}}\left[1 + \frac{C_c\left(2-c'_{f\mu}\right)}{4\pi kBP_{R_{\max}}}\sqrt{\frac{\phi\pi B\rho_{c,R_{\max}}}{\omega_{c,R_{\max}}\omega_{w,2w}M_c}}(R_{\max}-r)\right]^{\frac{2}{2-c'_{f\mu}}}, & R_c \le r < R_{\max} \\ P_0 + \frac{C_c}{2\pi kB\omega_{w,3}}\ln\frac{R_0}{r}, & R_{\max} \le r < R_0 \end{cases} \quad (41)$$

Note that Eq. (41) is similar to Eq. (20) of Wu et al. (2016). The essential difference is that only the partial miscibility of CO_2 and brine is included in the latter; however, the compressibility of fluid is also considered in the former, except that. To include the compressibility, the new definition for the coefficient of compressibility and the assumption of relative permeability both are very significant and available for multi-phase flow in porous media. In addition, the former belongs to the class of power function models, while the latter is an exponential function model.

As to the three characteristic radiuses in the reservoir, they are obtained by the following method. Letting $b = B$ and $b = 0$, R_c and $R_{\max}$ can be derived directly; that is,

$$R_c = \sqrt{\frac{\omega_{w,R_c}M_c}{\omega_{c,R_c}\phi\pi B\rho_{c,R_c}}},\ R_{\max} = \sqrt{\frac{\omega_{c,R_{\max}}M_c}{\omega_{w,R_{\max}}\phi\pi B\rho_{c,R_{\max}}}} \quad (42)$$

To obtain the characteristic radius R_0, the method of Wu et al. (2016) is adopted, as follows,

$$R_0 = \sqrt{\frac{4Ttu_0}{u^*}} + R_{\max} = \sqrt{\frac{4u_0kt}{\mu_w\phi(\alpha_p+\beta_w)}} + R_{\max} \quad (43)$$

where u^* is the storage coefficient of the porous medium; T is the transmissivity of the porous medium [L^2T^{-1}]; α_p,β_w are the traditional coefficient of compressibility of the pore and brine (water) [$ML^{-1}T^{-2}$], respectively; and u_0 is the zero of the well function, which corresponds to the outer boundary.

Table 3
The basic parameters used in the calculations related to Example 1.

Parameter	Value	Parameter	Value
r_{well} (m)	0.2	ρ_{c0} (kg/m^3)	723.68
B (m)	10	$c'_{f\rho}$	0.31
k (m^2)	$8*10^{-15}$	μ_{c0} (μPa·s)	60.042
P_0 (MPa)	20	$c'_{f\mu}$	0.58
ϕ	0.1	υ_{c0} (mm^2/s)	0.0829
α_p (1/Pa)	$4.5*10^{-10}$	$c'_{f\upsilon}$	0.27
β_w (1/Pa)	$4.5*10^{-10}$	υ_w (mm^2/s)	0.475
C_c (kg/s)	2	μ_w (μPa·s)	471.42

6. Application and verification

In this section, analyses of two typical examples are implemented to verify the reliability, improved nature and universality of the above advanced analytical solution for depicting the evaluation of fluid pressure in the reservoir. Specifically, it includes three aspects: (1) Comparison of the results calculated using the advanced analytical solution with simulated results from TOUGH2/ECO2N Pruess, 2005) to verify its reliability. ((2) Comparison of the results calculated using the advanced analytical solution with the results of previous analytical solution Wu et al., 2016) to verify that it represents an improvement. ((3) Application to two examples with differing reservoir characteristics to verify its universality. Example 1 represents a typical reservoir in the Shenhua CCS demonstration project, China, whose depth and temperature are approximately 2 km and 60 °C, respectively. It represents a reservoir with characteristics widely seen in China, including a small thickness and low permeability (Liu et al., 2013; Xie et al., 2015a; Xie et al., 2015b). The basic parameters used in the calculations are shown in Table 3. Example 2 is a standard example presented in the manual of TOUGH2/ECO2N. The depth and temperature of the reservoir are approximately 1.2 km and 45 °C, respectively. It is a quite typical reservoir and has characteristics that are seen all over the world, including a considerable thickness and high permeability (Bachu, 2003; Pruess, 2005). The basic parameters used in the calculations are shown in Table 4.

6.1. Example 1

For Example 1, in TOUGH2/ ECO2N, the cylindrical grids extend 50 km in the radial direction. We selected the Corey model to calculate the relative permeability, and the residual saturation of brine and CO_2 are 0.4 and 0.05, respectively. The capillary pressure is ignored, and 10,000 days of continuous CO_2 injection are simulated. The results calculated with this advanced analytical solution (Ana. Sol. 2 in figures) and the previous analytical solution (Ana. Sol. 1 in figures) and the

Table 4
The basic parameters used in calculations related to Example 2.

Parameter	Value	Parameter	Value
r_{well} (m)	0.3	ρ_{c0} (kg/m^3)	657.74
B (m)	100	$c'_{f\rho}$	0.27
k (m^2)	$1*10^{-13}$	μ_{c0} (μPa·s)	51.257
P_0 (MPa)	12	$c'_{f\mu}$	0.53
ϕ	0.12	υ_{c0} (mm^2/s)	0.0779
α_p (1/Pa)	$4.5*10^{-10}$	$c'_{f\upsilon}$	0.26
β_w (1/Pa)	$4.5*10^{-10}$	υ_w (mm^2/s)	0.600
C_c (kg/s)	100	μ_w (μPa·s)	597.77

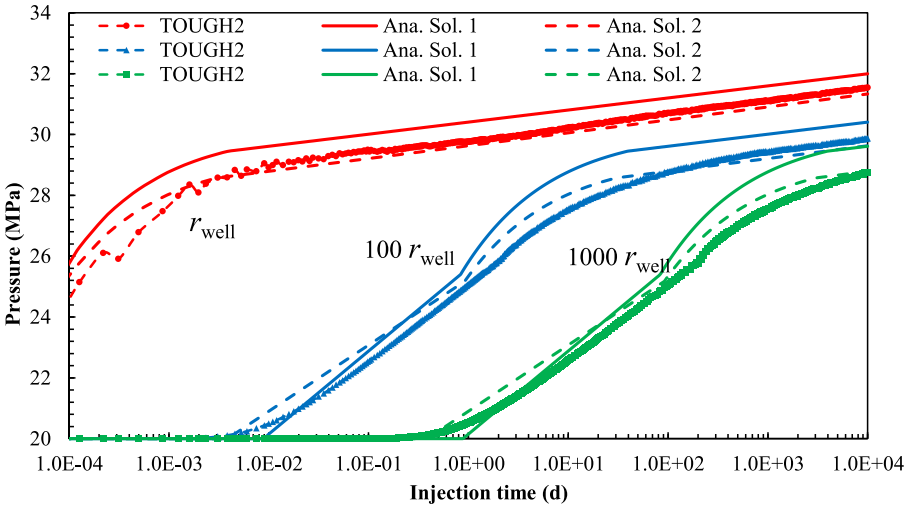

Fig. 4. Comparison of predicted fluid pressure profiles in the reservoir as a function of injection time for Example 1.

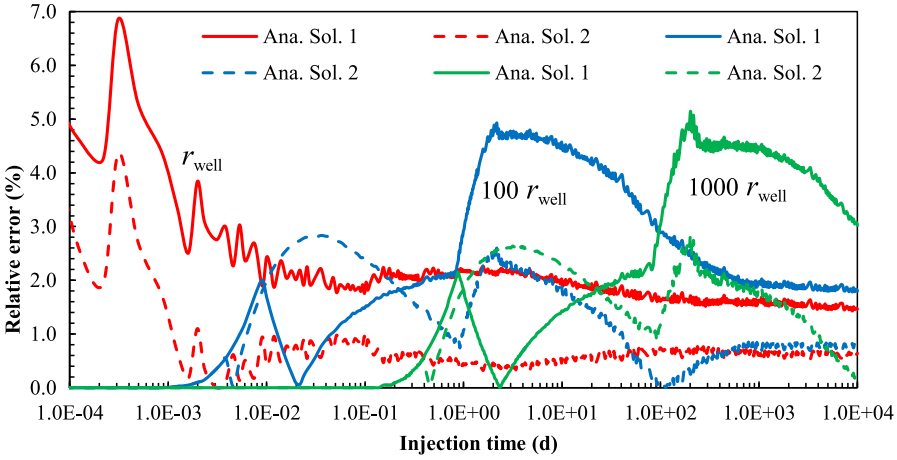

Fig. 5. Relative error of the analytical solutions as a function of injection time for Example 1.

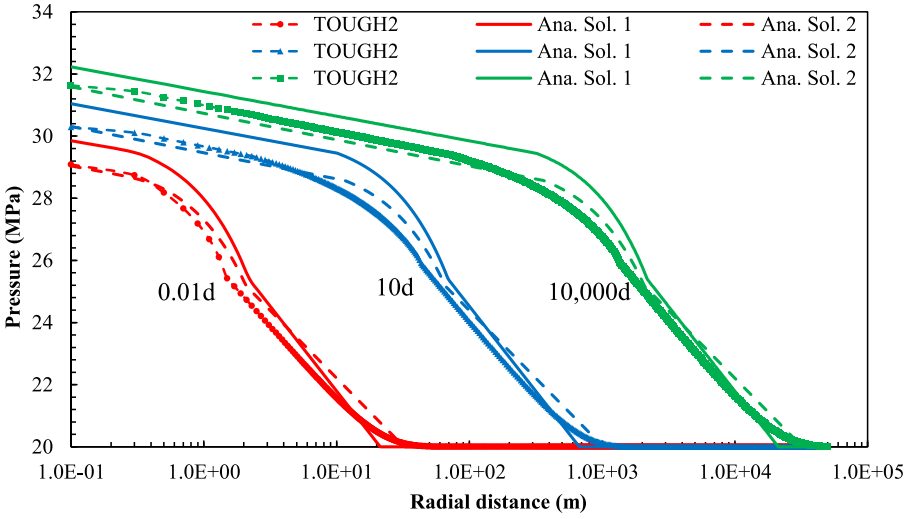

Fig. 6. Comparison of predicted fluid pressure profiles in the reservoir as a function of radial distance for Example 1.

simulated results from TOUGH2/ ECO2N (TOUGH2 in figures) are plotted in one figure. Figs. 4 and 6 show a comparison of predicted fluid pressure profiles at three different locations as a function of injection time, as well as a comparison of predicted fluid pressure profiles at three different moments as a function of radial distance, respectively. In addition, the corresponding relative error profiles of the analytical solutions are shown in Figs. 5 and 7.

It is clear from Figs. 4 and 6 that the fluid pressures predicted using the analytical solutions and the numerical solution have the same trend. The curves rise as injection time increases, while it decreases as radial distance increases. This result verifies the reliability of this advanced analytical solution. As shown in Figs. 5 and 7, the maximal relative error of the previous analytical solution exceeds 6%, whereas it is only 4% for the advanced analytical solution, and the relative error is mostly less than 3%. This result suggests that the analytical solution that includes the compressibility is more accurate and closer to actual conditions, so the

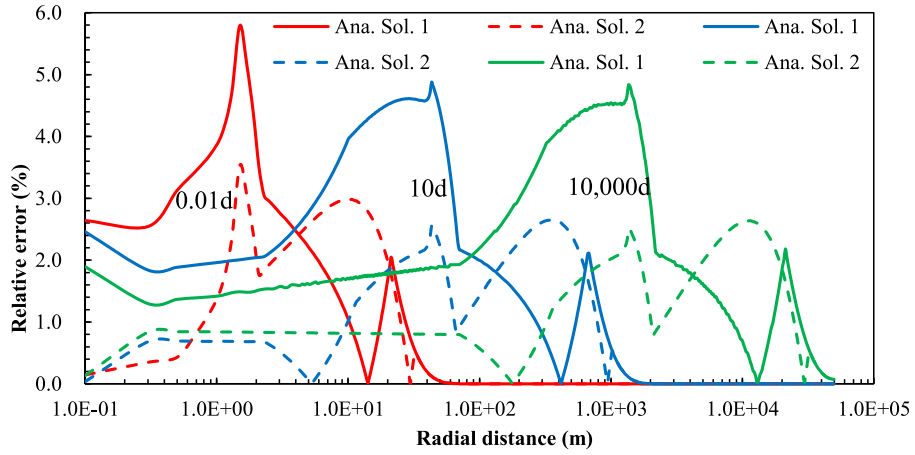

Fig. 7. Relative error of the analytical solutions as a function of radial distance for Example 1.

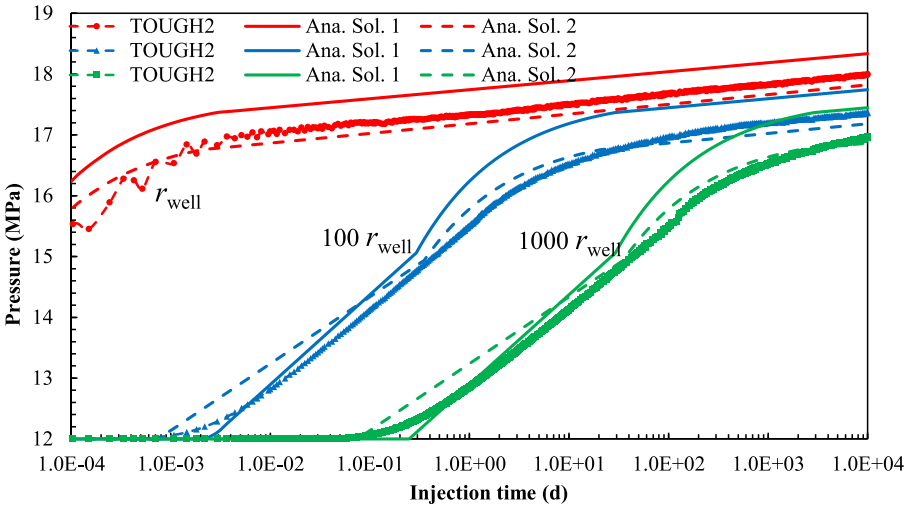

Fig. 8. Comparison of predicted fluid pressure profiles in the reservoir as a function of injection time for Example 2.

advancement represented by this work is clear. Furthermore, there are three turning points of pressure drop in the spatial distribution curves of pressure. Taking the results for 10 days as example, the three turning points are located at 11.46 m, 65.99 m and 1018.52 m, respectively. They are consistent with the three characteristic radiuses (R_c, R_{max} and R_0) in the reservoir at that moment. Therefore, it can be found from Fig. 6 that the rates of pressure decrease are constants in the gas source region and the region of drainage, while the rate of pressure decrease rises gradually in the region of displacement. In addition, the ordering of the three rates is: the region of displacement > the region of drainage > the gas source region. The results also indicate that the resistance to flow in the region of displacement is the largest, and it increases along the flow direction. Moreover, the resistance to flow of the single CO_2 phase is small. The main reasons are as follows. (1) The surface tension at the interface between the CO_2 and the brine is sufficiently large. (2) The viscosity of CO_2 is small. Moreover, from the perspective of relative error, the relative errors of the analytical solutions are greatest in the region of displacement, compared with the other two regions. This result indicates that the unsteady flow mainly occurs in the region of displacement, whereas steady flow occurs in the gas source region and the region of drainage. With increasing injection time, the ratio of the region of displacement to the other two regions becomes increasingly small, so the actual flow in the reservoir tends to gradually become quasi-steady.

6.2. Example 2

For Example 2, in TOUGH2/ECO2N, the differences in the parameter values used compared with Example 1 include two aspects. (1) The cylindrical grids extend 100 km in the radial direction, and (2) the residual saturation of the brine is 0.3. We use the same way to display the results, which are shown in Figs. 8–11. The conclusions drawn from Figs. 8–11 are consistent with those obtained from Figs. 4–7, which demonstrated that the advanced analytical solution is applicable in both of the two kinds of typical reservoirs. Thus, the universality of the advanced analytical solution is verified, and it is applicable all over the world.

7. Conclusions

To consider the compressibility of fluids, especially for CO_2, this work derived a new governing equation of describing the movement of complex fluids in reservoirs that is based on the equation of continuity and including the compressibility of fluid and Darcy's law generalized to multiphase flows. An advanced analytical solution about the evolution of fluid pressure was then obtained by integrating within different regions. Analyses of two typical examples verified the reliability, improved nature and universality of this new analytical solution, and it can be used in engineering applications all over the world.

To solve the problems associated with the traditional coefficient of compressibility, which cannot characterize the relationship between the physical properties of CO_2 and pressure, this work provided a more rigorous definition for the coefficient of compressibility of fluid, then derived the corresponding power function model (PFM). Comparison with a standard data base shows that the PFM is more accurate and applicable than the traditional exponential function model, verifying the reliability of the new definition.

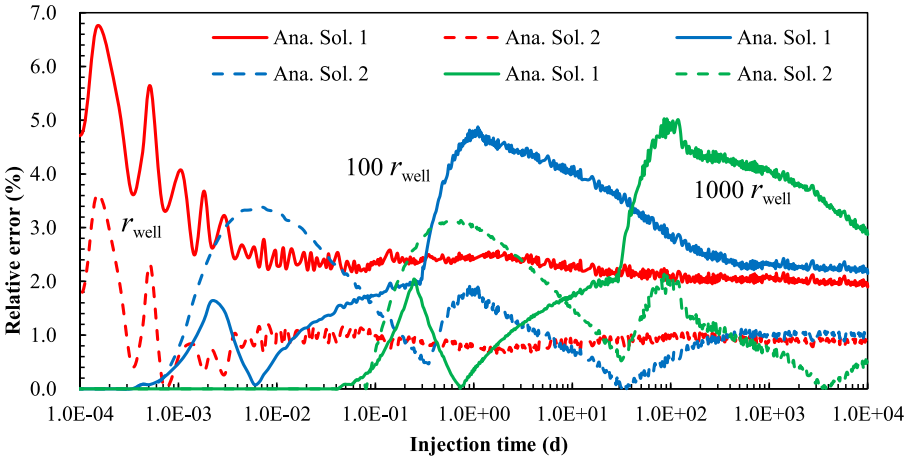

Fig. 9. Relative error of analytical solutions as a function of injection time for Example 2.

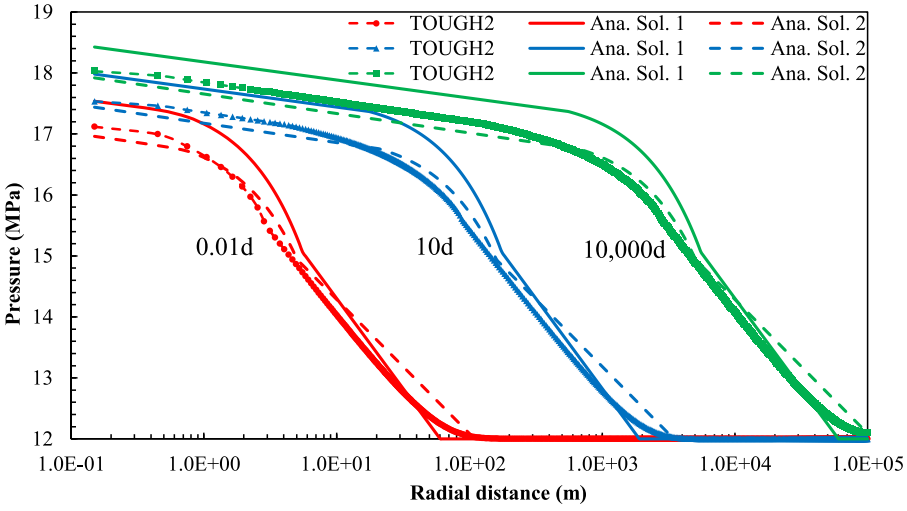

Fig. 10. Comparison of predicted fluid pressure profiles in the reservoir as a function of radial distance for Example 2.

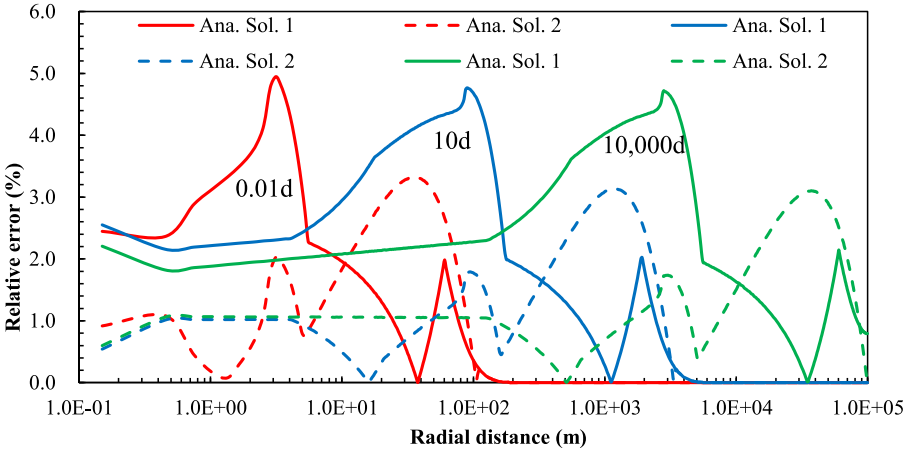

Fig. 11. Relative error of analytical solutions as a function of radial distance for Example 2.

Regarding the problem of difficulties in determining the saturation of fluids, a method of directly assuming the averaged relative permeability of each fluid phase in different fluid domains was proposed, according to the theory of gradual change. This method avoids the difficulties of determining the saturation of fluids and also eliminates the errors associated with the relative permeability models for risk assessment of reservoirs, improving the simulation accuracy.

According to the characteristics of the movement and distribution of complex fluids in reservoirs, this work divided the flow field into three regions. Ordered according to increasing radial distance, these regions are the gas source region, the region of displacement and the region of drainage. Moreover, unsteady flow is always present in the region of displacement, while steady flow occurs in the other two regions. With increasing injection time, the ratio of the region of displacement to the other two regions becomes increasingly small, so that the actual flow in the reservoir tends to gradually become quasi-steady.

The results of the sample calculations show that the surface tension at the interface between the CO_2 and the brine is sufficiently large that

the assumption of neglecting the capillary pressure induces a certain amount of error. It is worthwhile to investigate it in the future.

Acknowledgment

This work was sponsored by the Program of International Science and Technology Cooperation, China (Grant No. S2016G9005).

References

Alvarado, V., Manrique, E., 2010. Enhanced oil recovery: an update review. Energies 3 (9), 1529–1575.
Azizi, E., Cinar, Y., 2013. Approximate analytical solutions for CO2 injectivity into saline formations. Spe Reservoir Eval. Eng. 16 (2), 123–133.
Bachu, S., 2000. Sequestration of CO2 in geological media: criteria and approach for site selection in response to climate change. Energy Convers. Manage. 41.
Bachu, S., 2003. Screening and ranking of sedimentary basins for sequestration of CO2 in geological media in response to climate change. Environ. Geol. 44 (3), 277–289.
Bai, B., Li, X., Wu, H., Wang, Y., Liu, M., 2017. A methodology for designing maximum allowable wellhead pressure for CO2 injection: application to the Shenhua CCS demonstration project, China. Greenhouse Gases Sci. Technol. 7 (1), 151–181.
Blunt, M., King, P., 1991. Relative permeabilities from two- and three-dimensional pore-scale network modelling. Transp. Porous Media 6 (4), 407–433.
Buckley, S.E., Leverett, M.C., 1942. Mechanism of fluid displacement in sands. Trans. Am. Inst. Min. Metall. Pet. Eng. 146, 107–116.
Celia, M.A., Bachu, S., Nordbotten, J.M., Bandilla, K.W., 2015. Status of CO2 storage in deep saline aquifers with emphasis on modeling approaches and practical simulations. Water Resour. Res. 51 (9), 6846–6892.
Cihan, A., Birkholzer, J.T., Zhou, Q., 2013. Pressure buildup and brine migration during CO2 storage in multilayered aquifers. Ground Water 51 (2), 252–267.
Cooper, J., Stamford, L., Azapagic, A., 2016. Shale gas: a review of the economic, environmental, and social sustainability. Energy Technol. 4 (7), 772–792.
Damen, K., Faaij, A., van Bergen, F., Gale, J., Lysen, E., 2005. Identification of early opportunities for CO2 sequestration-worldwide screening for CO2-EOR and CO2-ECBM projects. Energy 30 (10), 1931–1952.
Dilmore, R.M., Allen, D., Pique, P., Jones, R.J., Hedges, S.W., Soong, Y., 2006. Experimental measurements of the solubility of CO2 in the brine of the Oriskany sandstone aquifer. In: 23rd Annual International Pittsburgh Coal Conference, Pittsburgh, PA, Sept. 25–28, 2006.
Fenghour, A., Wakeham, W.A., Vesovic, V., 1998. The viscosity of carbon dioxide. J. Phys. Chem. Reference Data 27 (1), 31–44.
Golding, S.D., Boreham, C.J., Esterle, J.S., 2013. Stable isotope geochemistry of coal bed and shale gas and related production waters: a review. Int. J. Coal Geol. 120, 24–40.
Gozalpour, F., Ren, S.R., Tohidi, B., 2005. CO2 EOR and storage in oil reservoirs. Oil Gas Sci. Technol.-Revue D Ifp Energ. Nouvelles 60 (3), 537–546.
IPCC, 2005. Carbon dioxide capture and storage. Intergovernmental Panel on Climate Change. WMO & UNEP, Cambridge University Press, New York.
Johns, R.T., Sah, P., Solano, R., 2002. Effect of dispersion on local displacement efficiency for multicomponent enriched-gas floods above the minimum miscibility enrichment. Spe Reservoir Eval. Eng. 5 (1), 4–10.
Kong, X., 2010. Gao Deng Shen Liu Li Xue, second ed. Science and technology of China Press, Hefai, pp. 808.
Lal, R., 2008. Sequestration of atmospheric CO2 in global carbon pools. Energy Environ. Sci. 1 (1), 86–100.
Li, C., Jia, W., Wu, X., 2012. Application of Lee-Kesler equation of state to calculating compressibility factors of high pressure condensate gas. In: Zeng, D. (Ed.), 2011 2nd International Conference on Advances in Energy Engineering, pp. 115–120.
Liu, H., Hou, Z., Were, P., Gou, Y., Sun, X., 2013. Simulation of CO2 plume movement in multilayered saline formations through multilayer injection technology in the Ordos Basin, China. Environ. Earth Sci. 71 (10), 4447–4462.
Lu, C., Han, W., Lee, S., Thorne, D., Esser, R., Mcpherson, B., 2008. Effects of density and mutual solubility of CO2-brine system on CO2 storage in geological formations. In: Paper presented at AGU Fall Meeting.
Mathias, S.A., Hardisty, P.E., Trudell, M.R., Zimmerman, R.W., 2009. Approximate solutions for pressure buildup during CO2 injection in brine aquifers. Transp. Porous Media 79 (2), 265–284.
Mathias, S.A., Gluyas, J.G., Gonzalez Martinez de Miguel, G.J., Hosseini, S.A., 2011a. Role of partial miscibility on pressure buildup due to constant rate injection of CO2 into closed and open brine aquifers. Water Resour. Res. 47 (12), 4154–4158.
Mathias, S.A., de Miguel, G.J.G.M., Thatcher, K.E., Zimmerman, R.W., 2011b. Pressure buildup during CO2 injection into a closed brine aquifer. Transp. Porous Media 89 (3), 383–397.
Michael, K., Golab, A., Shulakova, V., Ennis-King, J., Allinson, G., Sharma, S., Aiken, T., 2010. Geological storage of CO2 in saline aquifers-A review of the experience from existing storage operations. Int. J. Greenhouse Gas Control 4 (4), 659–667.
Mijic, A., LaForce, T.C., Muggeridge, A.H., 2014. CO2 injectivity in saline aquifers: the impact of non-Darcy flow, phase miscibility, and gas compressibility. Water Resour. Res. 50 (5), 4163–4185.
Nagy, S., Olajossy, A., 2008. Economic analysis of use of the early application CO2 and CO2/N-2-EOR technology in Poland. Arch. Mining Sci. 53 (1), 115–124.
NIST Chemistry WebBook: http://webbook.nist.gov/chemistry/, October 28, 2016.
Nordbotten, J.M., Celia, M.A., 2006a. An improved analytical solution for interface upconing around a well. Water Resour. Res. 42 (8).
Nordbotten, J.M., Celia, M.A., 2006b. Similarity solutions for fluid injection into confined aquifers. J. Fluid Mech. 561, 307–327.
Nordbotten, J.M., Celia, M.A., Bachu, S., 2005a. Injection and storage of CO2 in deep saline aquifers: Analytical solution for CO2 plume evolution during injection. Transp. Porous Media 58 (3), 339–360.
Nordbotten, J.M., Celia, M.A., Bachu, S., Dahle, H.K., 2005b. Semianalytical solution for CO2 leakage through an abandoned well. Environ. Sci. Technol. 39 (2), 602–611.
Poordad, S., Forutan, M.K., 2013. A review of the potential for CO2 sequestration and enhanced gas recovery in an Iranian gas condensate reservoir from a fluid properties point of view. Pet. Sci. Technol. 31 (20), 2157–2165.
Pruess, K., 2005. ECO2N: a TOUGH2 Fluid Property Module Formixtures of Water, NaCl, and CO2. Lawrence Berkeley National Laboratory Berkeley, Berkeley, CA.
Pruess, K., 2006. Enhanced geothermal systems (EGS) using CO2 as working fluid—a novel approach for generating renewable energy with simultaneous sequestration of carbon. Geothermics 35 (4), 351–367.
Pruess, K., Oldenburg, C.M., Moridis, G., 1999. TOUGH2 User's Guide, Version 2.0. Lawrence Berkeley National Laboratory Berkeley, Berkeley, CA.
Span, R., Wagner, W., 1996. A new equation of state for carbon dioxide covering the fluid region from the triple-point temperature to 1100 K at pressures up to 800 MPa. J. Phys. Chem. Reference Data 25 (6), 1509–1596.
Taber, J.J., Martin, F.D., Seright, R.S., 1997. EOR screening criteria revisited – Part 1: introduction to screening criteria and enhanced recovery field projects. Spe Reservoir Eng. 12 (3), 189–198.
Vesovic, V., Wakeham, W.A., Olchowy, G.A., Sengers, J.V., Watson, J.T.R., Millat, J., 1990. The transport-properties of carbon-dioxide. J. Phys. Chem. Reference Data 19 (3), 763–808.
Vilarrasa, V., Carrera, J., Bolster, D., Dentz, M., 2013. Semianalytical solution for plume shape and pressure evolution during injection in deep saline formations. Transp. Porous Media 97 (1), 43–65.
Vilarrasa, V., Bolster, D., Dentz, M., Olivella, S., Carrera, J., 2010. Effects of CO2 compressibility on CO2 storage in deep saline aquifers. Transp. Porous Media 85 (2), 619–639.
Wojnarowski, P., 2012. Potential for increasing oil recovery from Polish oil-fields by applying EOR methods. Gospodarka Surowcami Mineralnymi-Mineral Resour. Manage. 28 (4), 47–58.
Wu, H., Bai, B., Li, X., Gao, S., Liu, M., Wang, L., 2016. An explicit integral solution for pressure build-up during CO2 injection into infinite saline aquifers. Greenhouse Gases-Sci. Technol. 6 (5), 633–647.
Wu, H., Bai, B., Li, X., Liu, M., He, Y., 2017. An explicit finite difference model for prediction of wellbore pressure and temperature distribution in CO2 geological sequestration. Greenhouse Gases Sci. Technol. 7 (2), 353–369.
Xie, J., Zhang, K., Hu, L., Wang, Y., Chen, M., 2015a. Understanding the carbon dioxide sequestration in low-permeability saline aquifers in the Ordos Basin with numerical simulations. Greenhouse Gases 5 (5), 558–576.
Xie, J., Zhang, K., Hu, L., Pavelic, P., Wang, Y., Chen, M., 2015b. Field-based simulation of a demonstration site for carbon dioxide sequestration in low-permeability saline aquifers in the Ordos Basin, China. Hydrogeol. J. 23 (7), 465–1480.
Zyvoloski, G., 2007. FEHM: A control volume finite element code for simulating subsurface multi-phase multi-fluid heat and mass transfer. In: LA-UR-3359, Los Alamos.